This article has been accepted for publication in a future issue of this journal, but has not been fully edited. Content may change prior to final publication. Citation information: DOI 10.1109/JSEN.2018.2837159, IEEE Sensors Journal

Real time measuring system of multiple chemical parameters using microstructured optical fibers based sensors

A. Lopez-Aldaba, D. Lopez-Torres, C. Elosua, F.J. Arregui Member IEEE, J-L. Auguste, R. Jamier, P. Roy, and M. López-Amo Senior Member, IEEE

***Abstract*—In this paper, a multiplexing system for simultaneous interrogation of optical fiber sensors which measure different parameters is presented and validated. The whole system has been tested with 6 different sensing heads with different purposes: one temperature sensing head, two relative humidity sensors and three VOCs leak sensors; all of them based on microstructured optical fibers. The interrogation system uses the FFT technique to isolate each sensor's interference, enabling their simultaneous interrogation. The system interrogates all the sensors at frequencies up to 1 KHz, showing a good performance of each measurement without crosstalk between sensors. The developed system is independent of the sensors' purpose or of the multiplexing topology.**

***Index Terms*—Microstructured optical fiber, photonic crystal fiber, multiplexing, gas sensing.**

I. Introduction

MANY types of optical fibers have been used for sensing along the time: standard silica based, plastic, doped, and photonic crystal fibers are some examples. Since the first experiments with microstructured optical fibers (MOFs), they have shown relevant improved characteristics compared to conventional optical fibers as well as a great potential for sensing applications, overcoming some of the standard optical fiber handicaps [1], [2], [3]. Many geometries have been proposed for this kind of fibers. Among them, suspended-core MOFs present relatively large air holes surrounding a small core (typically a few microns diameter) resembling to be suspended along the fiber length but maintained by thin silica bridges. For instance, different pure silica suspended-core fibers have been used in temperature and curvature sensing [4], gas sensing [5], [6], [7], [8], [9], [10] micro-displacement measurements [11], refractive index [12], mechanical deformation [13] or biochemical sensing [14]. One of the most important type of MOF sensors are the ones based on evanescent field. These sensors have been used for different applications: simultaneous measurement of humidity and mechanical vibration [15], detection of biomolecules in aqueous solutions [16] as well as organic pollutants [17]. MOFs based sensors have also been utilized for gas measurements, like hydrogen detection [18], [19], methane [7] or acetylene [20]. However, long pieces of MOFs fibers and a pump to control this interaction are usually used in order to obtain a good interaction between gas and light. This configuration limits the utilization of these sensors in practical applications [21], [22].

Fiber based optical Fabry-Pérot (FP) interferometers are a quite popular sensor configuration due to their compactness, simple configuration, flexibility in tuning sensitivity and dynamic range. FP cavities composed by MOFs are also common structures: a hybrid structure formed by a MOF as the guiding fiber in cascade with a hollow-core fiber and a single mode fiber (SMF), was demonstrated for high-temperature sensing [23] among others [24]. Nitrogen sensors [25], chitosan based ones for relative humidity (RH) [26], [26], magnetic field [27], refractive index [28] as well as strain, temperature and pressure FP devices [29], [30] have been reported. Other fiber based sensors were implemented by fusing a small length of PCF to the end of a cleaved SMF for relative humidity ranged 40%-95% RH [31] or by chemical deposition of polymers [32].

In order to develop short, fast, sensitive and versatile FP-MOF sensors we have deposited thin films of different materials inside the MOFS. Nanocoated based sensors have recently experienced a remarkable development [33]. Furthermore, deposition techniques such as sputtering [34], [35], [36], [37], enable to control the morphology and thickness of the deposited coatings with high accuracy, and as a consequence, the final properties (sensitivity, kinetics) of the sensor.

Multiplexing interferometric sensors is a major target in the sensing field, allowing to perform multi-point and multi-parameter measurements within the scheme, and, therefore, reducing significantly the economic cost of the system. Multiplexing some Fabry-Pérot interferometric sensors without

This paragraph of the first footnote will contain the date on which you submitted your paper for review. Financial support from the Spanish Comisión Interministerial de Ciencia y Tecnología within projects TEC2016-76021-C2-1-R and TEC2016-78047-R, TEC2016-79367-C2-2-R. Cost action MP1401 and FEDER funds from the European Union are also acknowledged.

A. Lopez-Aldaba, D. Lopez-Torres, C. Elosua, F.J. Arregui and M. Lopez-Amo are with the Department of Electronic and Electronic Engineering and ISC, Universidad Publica de Navarra, E-31006 Pamplona, Spain (e-mail: aitor.lopez@unavarra.es; diego.lopez@unavarra.es; cesar.elosua@unavarra.es, parregui@unavarra.es; mla@unavarra.es).

J.-L. Auguste, R. Jamier and P. Roy are with the Fiber Photonics Department, UMR CNRS/University of Limoges 7252, 123 Avenue Albert Thomas, 87060 Limoges cedex, France (e-mail: jean-louis.auguste@xlim.fr; raphael.jamier@xlim.fr; philippe.roy@xlim.fr).

This article has been accepted for publication in a future issue of this journal, but has not been fully edited. Content may change prior to final publication. Citation information: DOI 10.1109/JSEN.2018.2837159, IEEE Sensors Journal

reflective layers present several difficulties due to their low reflectivity (4%) and their cavity length limitation (the number of multiplexed sensors depends on the cavity lengths chosen). Several approaches have been demonstrated during the last years: spatial-frequency-division multiplexing (SFDM) and coarse-wavelength-division multiplexing (CWDM) schemes [38], in-line FP cavities based on FBGs reflectometers [39], weak fiber Bragg gratings using frequency shifted interferometry [340], conventional graded-index multimode fibers in mode-multiplexed transmission [41], photonic crystal fibers in Sagnac interferometers [42] or polarization-division multiplexing [43]. These techniques present several handicaps such as complex setups with high economic cost or systems whose complexity increases exponentially with the number of multiplexed sensors.

In this paper, a multiplexing system with 6 FP-interferometric sensing heads for multiparameter monitoring is presented and characterized. In previous works, authors reported up to three sensors in a single optical channel for relative humidity measurements [44]. Using a commercial FBG interrogator with a MATLAB based software, six different RH sensors are simultaneously and independently measured within a single optical interrogator's channel. The scanning frequency of the commercial interrogator (from 1 Hz up to 1 KHz) allows real time measurements, avoiding the utilization of Optical Spectrum Analyzers and post-processing [45]. An experimental study of the sensors response and their crosstalk is presented by monitoring the Fast Fourier Transform (FFT) phase variations of the FP interference frequencies. This measuring method is independent of the signal amplitude and avoids the necessity of tracking the wavelength evolution in the spectrum, which becomes a problem when several interferometric contributions come up. Also, the multiplexing system is independent of the monitoring target of each interferometric sensor. Thus with the FFT method it is possible to multiplex sensors in real time for multiple purposes (even vibrations at frequencies higher than the scanning frequency of the interrogation system [15]) without crosstalk.

The sensors based on MOF-FP cavities had been reported previously by ourselves, but it is the very first time we report in a journal the multiplexing of these MOF-FP cavities for different chemical parameters´ detection with different deposited materials with these promising results in terms of sensitivity and fast response time. This proof of concept validates the utilization of these sensors for applications such as electronic noses [46] or Toxic and Hazardous Gas Detection [47, 48].

II. Materials & Methods

In this work, 6 different sensors were fabricated and multiplexed within a single optical interrogator channel as shown in Fig. 1. To multiplex all the sensors, 3 optical couplers were used in cascade in order to achieve the required number of multiplexing channels. In this particular case, in a first stage, a 2x4 optical coupler was used to divide the optical interrogator's output in 4 identical optical paths. 2 of this paths were directly used with two sensors and the others were used as inputs in a second multiplexing stage where 2 2x2 optical couplers were installed. All the output channels of the 2x2 couplers were directly connected to their corresponding sensing head.

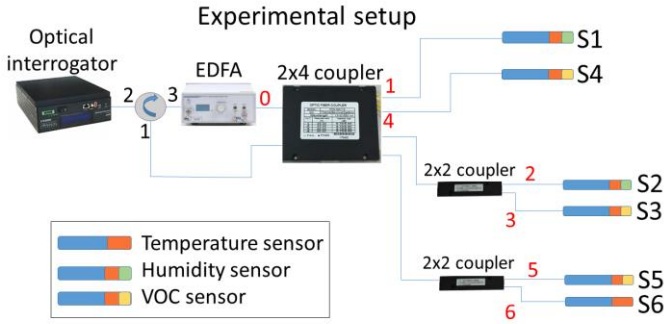

Fig. 1. Multiplexing experimental setup.

The sensor's distribution was chosen in relation with their optical insertion losses. Sensors S1 and S4 presented higher optical losses and therefore they were directly connected to the 2x4 optical interrogator's output. Sensors S2, S3, S5 and S6 were connected to the outputs of the 2x2 couplers.

The optical losses of the multiplexing system where measured before installing the sensors and results are shown in Table 1. Optical ports are highlighted in red color in Fig. 1, being port 0 the input port of the multiplexing system and port 1, 2, 3, 4, 5 and 6 the corresponding port of each sensing head.

Table 1. Optical losses between optical ports.

Ports	Optical losses (dB)
0 → 1	6.55
0 → 2	10
0 → 3	10.87
0 → 4	7.15
0 → 5	11.15
0 → 6	10.6

As it can be remarked from Table 1, ports 1 and 4 were the most suitable ones for the sensing heads with higher optical losses.

Six Fabry-Perot based sensing heads were multiplexed and used as sensors in this work. These cavities were made from a microstructured optical fiber with particular characteristics. The MOF used was fabricated using the stack and draw process. It is formed by four large air holes divided by four bridges, presenting a suspended core of 6.5 μm by 806 nm exhibiting a double Y shape, as it was studied in [49]. The Fabry-Pérot cavities were made by splicing different lengths of MOF fiber to one side of a single mode fiber (Corning SMF-28). The splice was made with a Fitel S175 fusion splicer with a custom developed program for this MOF and manual operation for its alignment. This manual splice leads to different insertion losses in each sensing head that must be taken into account.

By splicing a piece of MOF to a SMF, two low-reflectivity mirrors are formed at both ends of the MOF: the first one in the interface SMF-MOF due to the discontinuity in refractive index between both fibers; the second one is located at the interface

MOF-air because this high discontinuity provides a Fresnel reflection (3.3%). As a result, a low-finesse Fabry-Pérot interferometer is created when a light beam reaches the cavity (MOF) and it is reflected between the two interfaces several times. Each beam has a certain phase difference with respect to the preceding one: this shift corresponds to the extra path length travelled inside the cavity. Due to the high loss of the MOF and the low reflectivity of the air-glass interface, high order reflections inside the cavity are neglected and therefore a low-finesse scenario is assumed, which approximates a two-beam Fabry-Perot [50]. Furthermore, and for the same reasons, high order modes influence is negligible as they propagate, presenting an optical power one order of magnitude lower compared with the fundamental one.

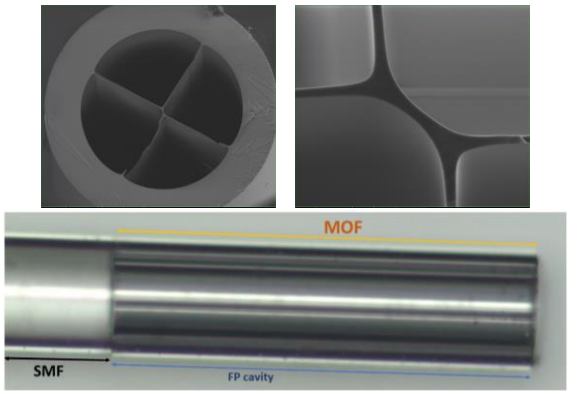

Fig. 2. MOF-4-Bridge cross section (SEM picture) and a resulting FP cavity (microscope picture).

Assuming a two beam Fabry-Perot, the reflected signal obtained should follow equation (1), where $\Delta\lambda$ is the optical spectrum wavelength spacing, λ is the working wavelength, n is the refractive index (neff = 1.37 [49]) and d is the MOF cavity length.

$$\Delta\lambda = \lambda^2/2nd \quad (1)$$

Two commercial interrogators of optical fiber sensors (Smartec SM125 and Smartec Si155) were used to illuminate the network and also to analyze the spectra signals guided through the MOF sensors. The optical interrogators employed were originally commercialized for FBG sensors´ monitoring and allow sensors to be interrogated with a scan frequency of 1 Hz and a 5 pm resolution for the SM125 and 1k Hz and 10pm for the Si155. Si155 optical interrogator allowed the system performance to be verified in high sampling frequency conditions being possible to take measures up to 1k Hz. FFT is computed in MATLAB also every sample, providing real-time information of the sensor system [51].

The FFT technique allows each sensor to be monitored independently avoiding the noise influence (high frequency components in the FFT module) or signal amplitude variations (variations in the power of the FFT module).

We want to remark that this interrogation method can be used in any of the usual topologies of optical fiber sensors multiplexing networks (star, tree, bus, mesh…[52]). These typical multiplexing networks prefer bus topologies in order to save cabling costs. However, these systems require complicated modulation/demodulation techniques and fiber delays to identify each interferometric sensor [53] or FBGs placed by the sensors to identify them [54]. Our interrogation method is also suitable for this kind of topology because the sensors´ identification is achieved in the spatial frequency domain and not by their position inside the networks, as happens in time division multiplexing (TDM) modulated systems.

Due to the optical losses of the sensing heads and the multiplexing system, a pre-amplification stage was used. The objective of this amplification stage is to compensate all the induced losses and to allow long distance remote motorization (up to 75km with the sensors comprised in this work). This stage is composed of a 3 port optical circulator and an Erbium doped amplifier (EDFA). The optical circulator is needed in order to use the same optical interrogator's channel to send and collect the light into and from the multiplexing system.

In order to verify the performance of the multiplexing system and the polyvalence of its combination with this type of sensing heads, three kind of sensors were employed: one temperature sensor, two relative humidity sensors and three volatile organic compounds presence sensors.

Relative humidity sensors were developed by creating a thin film of SnO2 inside the holes of the MOF fiber through the sputtering process, as authors previously demonstrated in [55]. VOCs presence sensors were developed with the same technique but changing the sensing material to ITO [56]. Temperature sensor is the FP-MOF cavity without any deposited sensitive layer [49]. These thin film depositions do not vary the interference period of the sensing heads but reduce their amplitude depending on the deposition time.

Deposition time determines the sensor's performance (sensitivity and response time). In this work, the deposition time of each sensor has been selected in order to enable simultaneous measurement in the same atmosphere avoiding crosstalk between sensors. For this reason, their sensitivity is not maximal when compared with the results showed in [46], [55], [56], as they were optimized.

The interaction between SnO_2/ITO and H_2O/VOCs molecules is due to a phenomena called chemisorption by means of the adsorption/desorption of these molecules [57].

S1 and S2 present a SnO_2 thin film sensitive layer as a result of a 2 minutes sputtering process. S3, S4 and S5 have an ITO thin film sensitive. This metallic oxide changes its refractive index in presence of different VOCs. Thus, an ITO thin film was deposited onto the head and into the walls of the MOF using a sputtering technique. The distance between the target of ITO and the head of the sensor was set at 5 cm. The main transduction mechanism which governs the behavior of this sensor [58] is the interaction between the evanescent field of the guided light along the MOF and the ITO thin film deposited into the walls of the MOF.S6 presents no sputtering deposition in order to keep it insensible to relative humidity nor VOCs variations.

External variations (in the example studied: temperature, relative humidity or VOCs presence for each kind of sensing head) produce a wavelength shift in the optical spectrum domain. In the FFT domain, this shift is translated into a variation of the FFT phase of the corresponding FFT module

This article has been accepted for publication in a future issue of this journal, but has not been fully edited. Content may change prior to final publication. Citation information: DOI 10.1109/JSEN.2018.2837159, IEEE Sensors Journal

delta. By monitoring the FFT phase of each sensors' main component, optical wavelength variations can be unambiguously identified.

To perform the temperature and relative humidity measurements, sensors were inserted inside a climatic chamber (Binder KMF 115). VOC presence was tested by introducing the sensors in fully saturated methanol atmospheres.

III. RESULTS & DISCUSSION

A. Multiplexing system

The FFT technique allows to multiplex a number of sensors using the whole spectral range for each of them. Each sensor presents a sinusoidal interference pattern in the optical spectrum domain.

As can be seen in equation (1) the MOF cavity length determines its interference wavelength spacing period ($\Delta\lambda$). Different sensors were obtained varying this interference period, as shown in Table 2.

Table 2. Cavity lengths and their associated interference periods.

Sensor	MOF Cavity Length (mm)	$\Delta\lambda$ (nm)
S1	~1.25	0.7
S2	~0.8	1.1
S3	~0.4	2.2
S4	~1.4	0.63
S5	~0.7	1.28
S6	~0.65	1.35

The individual optical spectra of the sensors mentioned above are shown in Fig. 3. These MOF cavity lengths were chosen in order to get examples of sensors in a wide spatial frequency range (0.4 – 1.5 nm^{-1}) and also to verify their performance when other sensors are located in a spatial frequency close to them.

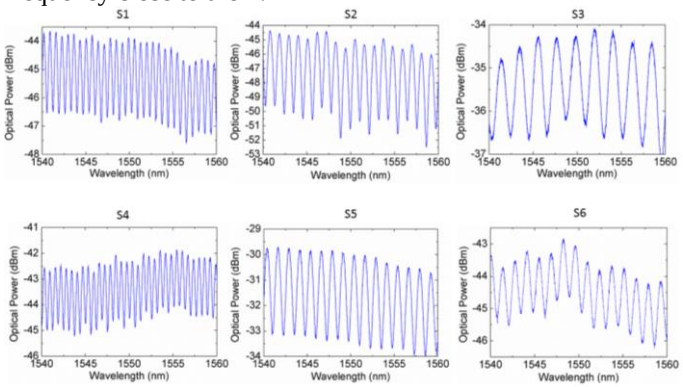

Fig. 3. Sensor's individual optical spectrum.

Using the setup showed in Fig. 1, the resulting optical spectrum is shown in Fig. 4. This optical spectrum is the result of the combination of all the sensor's interferences. As can be noticed, it becomes impossible to track the evolution of each interference independently and a wavelength shift in one of the interferences produces a wavelength variation of the whole multiplexed optical spectrum.

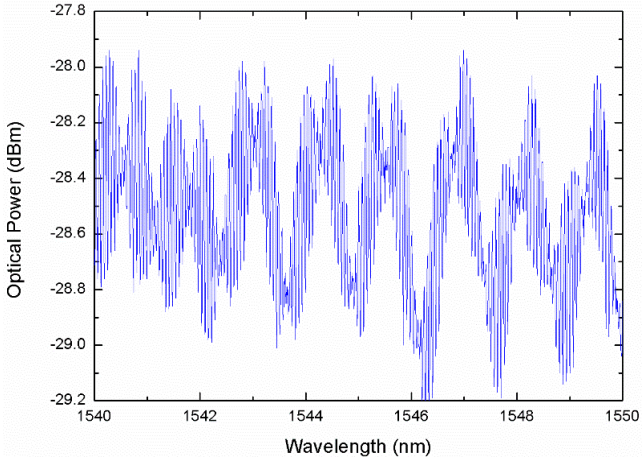

Fig. 4. Resulting multiplexed optical spectrum.

Typically, interferometric sensors have been multiplexed through wavelength division multiplexing devices (WDM) [59], [60] committing a certain wavelength range for each sensor. This technique allows a low number of sensors to be multiplexed, depending on the wavelength range committed to each sensor and the operating wavelength range of the devices employed (light source, analyzer and EDFA). Moreover, the interference period ($\Delta\lambda$) of each sensor and the wavelength range assigned to it determines the operating range of the device, leading to a tradeoff between operating range of the sensor and the number of sensors that can be multiplexed.

The FFT of each optical spectrum leads to a single peak (theoretically a single Dirac delta) in the FFT magnitude domain as can be seen in Fig. 5. The experimental FFT magnitude of each sensor is shown in Fig. 5. Table 2 show the theoretical frequencies that should be obtained just by applying equation (2), where x makes reference to any sensor.

$$Freq_x = 1/\Delta\lambda x \quad (2)$$

Table 3. FFT frequencies of each sensor.

Sensor	$\Delta\lambda$ (nm)	FFT frequency (nm^{-1})
S1	0.7	~1.43
S2	1.1	~0.9
S3	2.2	~0.45
S4	0.63	~1.59
S5	1.28	~0.78
S6	1.35	~0.74

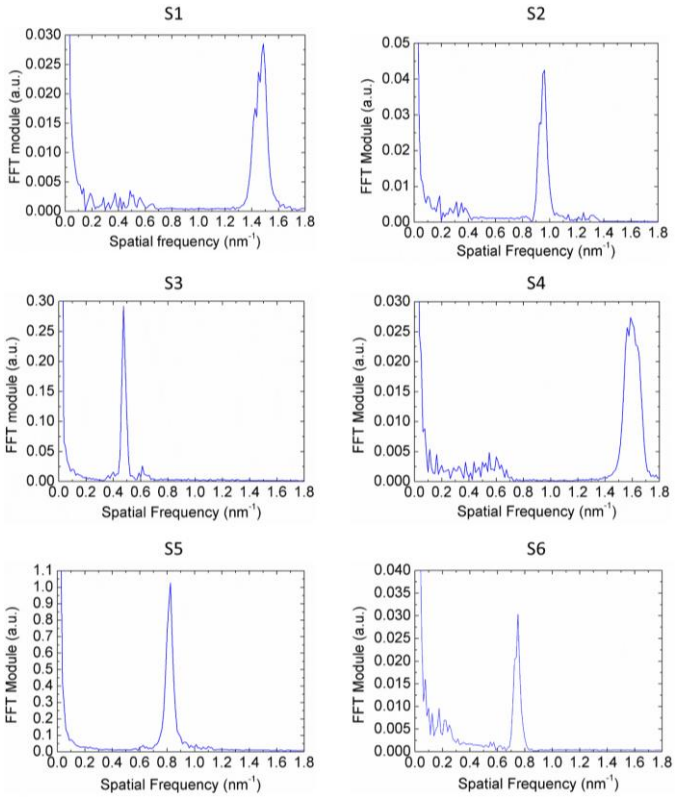

Fig. 5. Sensor's individual FFT magnitude.

As can be seen in Fig. 5 theoretical frequencies matches with experimental FFT results of each sensors. With this technique, the experimental multiplexed FFT magnitude is shown in Fig.6.

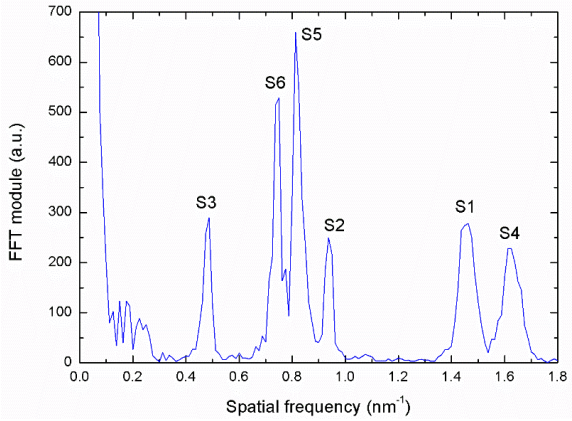

Fig. 6. Multiplexed FFT magnitude spectrum.

The FFT shows two single Dirac deltas in the FFT module domain (one in the negative part of the FFT spectrum and one in the positive part) due to the sinusoid optical spectrum resulting of each MOF-FP cavity. Experimentally, it is not a perfect Dirac delta but a broadened component because of the limited number of samples in each period of the optical interference the FFT. This is due to the FFT properties: the more samples are comprised within an optical spectrum interference period, the most defined will be the FFT delta. As a result, the higher the interference period is, the more number of points are comprised within it and therefore the resulting FFT delta is more defined. As an example, S3 presents an interference period of 2.2 nm which means 440 samples (optical interrogator's resolution of 05pm) and then, S4 has an interference period of 0.63 nm which means 126 samples. This property involves a technical limit of the maximum number of sensors that can be multiplexed in a single channel.

B. Multiplexing system validation

A scenario of 6 sensing heads for temperature, relative humidity and methanol presence was designed to test the performance of the multiplexing system and verify its capability to multiplex several sensors with independence of their sensing target. As presented in Fig. 1, S1 and S2 monitored temperature variations, S3, S4 and S5 were developed to monitor methanol presence and S6 monitored temperature variations. The objective of the system is to be able to monitor each sensor independently of the others and without crosstalk between them.

1) Temperature monitoring

FP-MOF based temperature sensors are fully described in [49].

In this case, all sensors are sensitive to temperature variations as all of them are made of a MOF-FP cavity [49]. In order to avoid this temperature crosstalk, a temperature characterization was carried out as shown in Fig. 7.

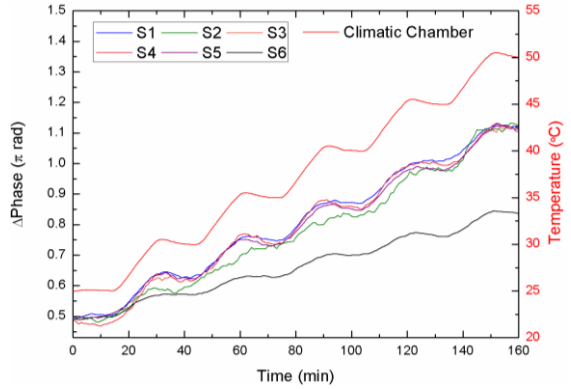

Fig. 7. Temperature characterization of all the sensors.

In order to avoid the temperature influence in sensors S1-S5, S6 is used as temperature reference. For these measurements, S6 was inserted inside the climatic chamber and the other were placed in a box outside. All the sensors were monitored simultaneously using the multiplexing setup. Temperature variations from 25ºC to 50ºC were applied to only S6 with 5ºC steps as Fig. 8 illustrates.

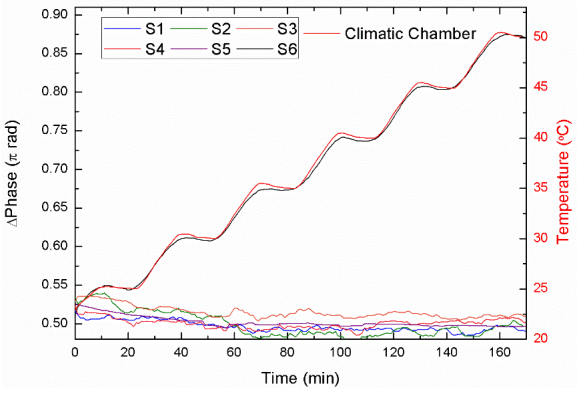

Fig. 8. S6 performance towards temperature variations.

This article has been accepted for publication in a future issue of this journal, but has not been fully edited. Content may change prior to final publication. Citation information: DOI 10.1109/JSEN.2018.2837159, IEEE Sensors Journal

As can be noticed, S6 works as temperature sensor showing a sensitivity of 0.015π rad/ºC. S1, S2, S3, S4 and S5 are not affected by temperature variations inside the climatic chamber verifying the systems isolation capability. They show small variations due to room temperature variations of ±0.4ºC, but with no relation to the steps induced by the climatic chamber.

Knowing all sensors´ temperature sensitivities and being S6 insensitive to relative humidity and to VOCs concentration variations, this last sensor is used as a temperature reference, making consequently the system independent from temperature variations by means of the suitable calibration algorithm.

2) Relative humidity monitoring

SnO_2-FP-MOF based relative humidity sensors are fully described in [49]. S1 and S2 were deposited with a ~2 minutes SnO2 sputtering deposition. Firstly, S1 was inserted inside the climatic chamber while S2, S3, S4, S5 and S6 remained outside in an expanded polystyrene EPS box to avoid the room temperature variations influence. All sensors were monitored simultaneously. The results of this experiment are shown in Fig. 9. Secondly, S2 was placed inside the climatic chamber and S1, S3, S4, S5 and S6 inside the box. As previously all sensors were monitored at the same time which results are shown in Fig. 10.

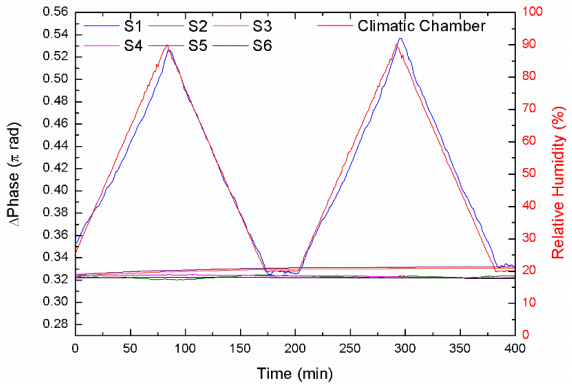

Fig. 9. S1 performance towards relative humidity variations.

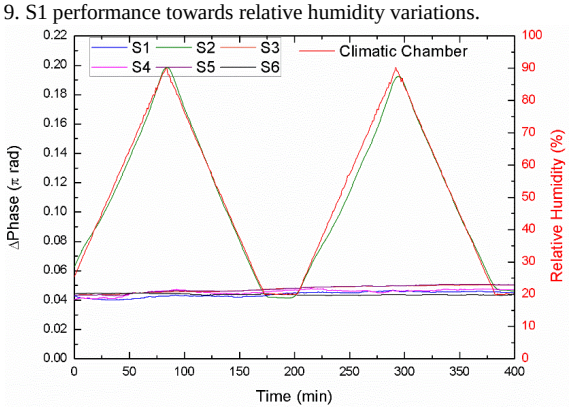

Fig. 10. S2 performance towards relative humidity variations.

Both sensors showed good agreement with climatic chamber's variations and presented no crosstalk with sensors outside it. A little hysteresis effect can be seen in S1: it might be caused by the carton substrate used to fix the sensors as it retains water molecules easily. S1 and S2 showed sensitivities of 0.003π rad/% RH and 0.0021π rad/% RH respectively. This sensitivity difference is due to the difference in the sensitive layers thickness. S3, S4 and S5 also showed low sensitivities towards humidity variations as ITO also reacts towards this parameter but their sensitivities are 10 times lower than S1 and S2. S6 is insensitive towards humidity variations.

Moreover, different approaches have been developed in order to make more selective this kind of sensors like the use of post process techniques as for example "principal component analysis" (PCA) [61], artificial neural networks [62] or making more selective the sensing layer using other metals or additives [63].

3) VOC (methanol) presence monitoring

The sensing material selected was ITO because it has been previously used to successfully detect VOCs.

Fig. 11 shows all the system performance when S3 is exposed to fully saturated atmospheres of methanol. As in previous analysis, all sensors were monitored simultaneously. Fig. 12 and Fig. 13 illustrates the systems results when S4 and S5 respectively are exposed to methanol atmospheres.

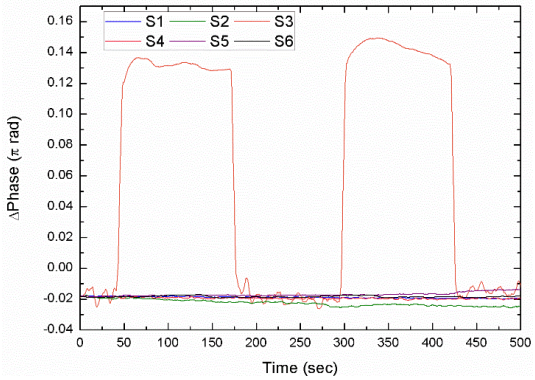

Fig. 11. S3 performance towards methanol fully saturated atmosphere.

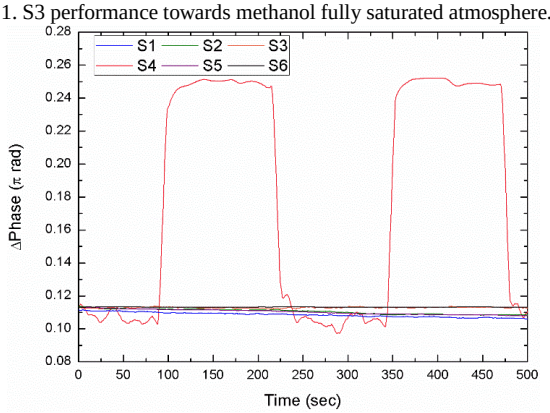

Fig. 12. S4 performance towards methanol fully saturated atmosphere.

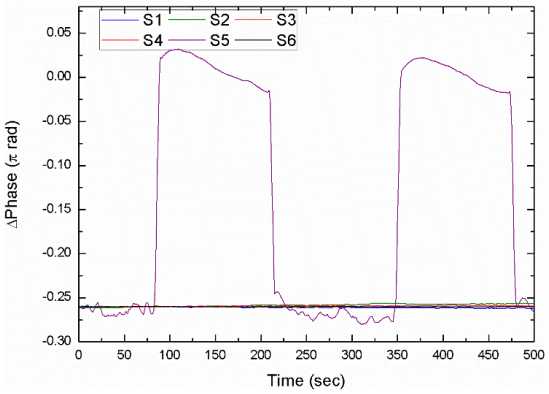

Fig. 13. S5 performance towards methanol fully saturated atmosphere.

As in previous results, the sensors exposed showed sensitivity to methanol presence and the others presented no

crosstalk between them. With the deposition times presented, sensors showed maximal phase shifts of 0.15π rad, 0.16π rad and 0.31π rad respectively, making them suitable for escape detectors in gas bottles or containers applications.

Analogously, as it happened with humidity measurements, S1 and S2 presents low sensitivity towards methanol in comparison with S3, S4 and S5. S6 is insensitive towards methanol variations. Due to this important sensitivities difference, using one sensor as reference, this crosstalk influence can be reduced.

Taking into account all the results obtained during the experiments, the system can be used to multiplex interferometric sensors without crosstalk between them. Additionally, a multipoint application to monitor temperature, relative humidity and VOCs escapes with 6 sensing heads has been presented and characterized. The multiplexing system can be used with any combination of sensors and applications and an example has just been presented.

IV. CONCLUSION

In summary, a multiplexing system for interferometric sensors based on the FFT has been presented and validated. Six sensing heads have been multiplexed and measured simultaneously within a single channel of an optical interrogator showing no crosstalk between sensors. The measurements have been carried out by measuring the phase of the FFT component of each sensor at a scanning frequency from 1 Hz up to 1 KHz. The number of multiplexed sensors depends on the Fabry-Perot cavity lengths chosen.

An application for temperature, relative humidity and Volatile Organic Compounds has been proposed and analyzed. Sensors sensitivity depends on the deposited thin film material and deposition time. One sensor is proposed for temperature measurements, two sensors for relative humidity (20-90%) and three sensors for methanol presence. All of them show great sensitivity to their parameter target and no crosstalk between sensors.

This multiplexing technique is independent of the measured parameter by the MOF based sensors and also of the topology of the multiplexing network.

REFERENCES

[1] A. M. R. Pinto and M. Lopez-Amo, 'Photonic Crystal Fibers for Sensing Applications', *J. Sensors*, vol. 2012, pp. 1–21, 2012.

[2] T. M. Monro, S. Warren-Smith, E. P. Schartner, A. Franois, S. Heng, H. Ebendorff-Heidepriem, and S. Afshar, 'Sensing with suspended-core optical fibers', *Opt. Fiber Technol.*, vol. 16, no. 6, pp. 343–356, 2010.

[3] O. Frazão, J. L. Santos, F. M. Araújo, and L. A. Ferreira, 'Optical sensing with photonic crystal fibers', *Laser Photonics Rev.*, vol. 2, no. 6, pp. 449–459, 2008.

[4] O. Frazão, S. F. O. Silva, J. Viegas, J. M. Baptista, J. L. Santos, J. Kobelke, and K. Schuster, 'All fiber MachZehnder interferometer based on suspended twin-core fiber', *IEEE Photonics Technol. Lett.*, vol. 22, no. 17, pp. 1300–1302, 2010.

[5] A. S. Webb, 'Suspended-core holey fiber for evanescent-field sensing', *Opt. Eng.*, vol. 46, no. 1, p. 10503, 2007.

[6] L. Niu, C. Zhao, L. Qi, C. C. Chan, J. Kang, S. Jin, J. Guo, and H. Wei, 'Photonic Crystal Fiber Loop Mirror-Based', vol. 32, no. 22, pp. 4416–4421, 2014.

[7] Y. L. Hoo, S. Liu, H. L. Ho, and W. Jin, 'Fast response microstructured optical fiber methane sensor with multiple side-openings', *IEEE Photonics Technol. Lett.*, vol. 22, no. 5, pp. 296–298, 2010.

[8] V. P. Minkovich, , D. Monzón-Hernández, J. Villatoro, and G. Badenes, 'Microstructured optical fiber coated with thin films for gas and chemical sensing', *Optics Express*, vol. 14, no 18, p. 8413-8418, 2006.

[9] J. Villatoro, M. P. Kreuzer, R. Jha, V. P. Minkovich, V. Finazzi, G. Badenes, and V. Pruneri, 'Photonic crystal fiber interferometer for chemical vapor detection with high sensitivity', Optics Express, vol. 17, no. 3, pp. 1447-1453, 2009.

[10] S. Olyaee, A. Naraghi, and V. Ahmadi, 'High sensitivity evanescent-field gas sensor based on modified photonic crystal fiber for gas condensate and air pollution monitoring', Optik-International Journal for Light and Electron Optics, vol. 125, no. 5, pp. 596-600, 2014.

[11] M. Bravo, A. M. R. Pinto, M. Lopez-Amo, J. Kobelke, and K. Schuster, 'High precision micro-displacement fiber sensor through a suspended-core Sagnac interferometer', *Opt. Lett.*, vol. 37, no. 2, p. 202, 2012.

[12] J. Tian, Z. Lu, M. Quan, Y. Jiao, and Y. Yao, 'Fast response Fabry–Perot interferometer microfluidic refractive index fiber sensor based on concave-core photonic crystal fiber', *Opt. Express*, vol. 24, no. 18, p. 20132, 2016.

[13] R. O. A. B. Eiu, V. A. B. Eiu, and V. I. L. D. Uma, 'Fiber optic mechanical deformation sensors employing perpendicular photonic crystals', vol. 25, no. 19, pp. 23388–23398, 2017.

[14] L. Rindorf, J. B. Jensen, M. Dufva, L. H. Pedersen, P. E. Høiby, and O. Bang, 'Photonic crystal fiber long-period gratings for biochemical sensing.', *Opt. Express*, vol. 14, no. 18, pp. 8224–8231, 2006.

[15] S. Rota-Rodrigo, A. López-Aldaba, R. A. Pérez-Herrera, M. Del Carmen López Bautista, O. Esteban, and M. López-Amo, 'Simultaneous measurement of humidity and vibration based on a microwire sensor system using fast fourier transform technique', *J. Light. Technol.*, vol. 34, no. 19, pp. 1–6, 2016.

[16] J. B. Jensen, L. H. Pedersen, P. E. Hoiby, L. B. Nielsen, T. P. Hansen, J. R. Folkenberg, J. Riishede, D. Noordegraaf, K. Nielsen, a Carlsen, and a Bjarklev, 'Photonic crystal fiber based evanescent-wave sensor for detection of biomolecules in aqueous solutions.', *Opt. Lett.*, vol. 29, no. 17, pp. 1974–1976, 2004.

[17] J. Bürck, J. P. Conzen, and H. J. Ache, 'A fiber optic evanescent field absorption sensor for monitoring organic contaminants in water', *Fresenius. J. Anal. Chem.*, vol. 342, no. 4–5, pp. 394–400, 1992.

[18] M. Tabibazarp, B. Sutapun, R. Petrick, and A. Kazemi, 'Fiber Optics With Exposed Cores and Evanescent Field Interactions', vol. 3513, pp. 80–88, 1998.

[19] S. Sekimoto, H. Nakagawa, S. Okazaki, K. Fukuda, S. Asakura, T. Shigemori, and S. Takahashi, 'Fiber-optic evanescent-wave hydrogen gas sensor using palladium-supported tungsten oxide', *Sensors Actuators, B Chem.*, vol. 66, no. 1, pp. 142–145, 2000.

[20] G. F. Yan, A. P. Zhang, G. Y. Ma, B. H. Wang, B. Kim, J. Im, S. L. He, and Y. Chung, 'Fiber-Optic Acetylene Gas Sensor Based on Microstructured Optical Fiber Bragg Gratings', *Ieee Photonics Technol. Lett.*, vol. 23, no. 21, pp. 1588–1590, 2011.

[21] M. Cubillas, M. Silva-Lopez, J. M. Lazaro, O. M. Conde, M. N. Petrovich, and J. M. Lopez-Higuera, 'Methane detection at 1670-nm band using a hollow-core photonic bandgap fiber and a multiline algorithm.', *Opt. Express*, vol. 15, no. 26, pp. 17570–17576, 2007.

[22] T. Ritari, J. Tuominen, H. Ludvigsen, J. C. Petersen, T. Sorensen, T. P. Hansen, and H. R. Simonsen, 'Gas sensing using air-guiding photonic bandgap fibers', *Opt. Express*, vol. 12, no. 17, p. 4080, 2004.

[23] H. Y. Choi, K. S. Park, S. J. Park, U. C. Paek, B. H. Lee, and E. S. Choi, 'Miniature fiber-optic high temperature sensor based on a hybrid structured Fabry-Perot interferometer', *Opt. Lett.*, vol. 33, no. 21, pp. 2455–2457, 2008.

[24] C. Wu, H. Y. Fu, K. K. Qureshi, B. O. Guan, and H. Y. Tam, 'High-pressure and high-temperature characteristics of a Fabry–Perot interferometer based on photonic crystal fiber', Optics letters, vil. 36, no. 3, pp. 412-414, 2011

[25] G. Z. Xiao, A. Adnet, Z. Zhang, F. G. Sun, and C. P. Grover, 'Monitoring changes in the refractive index of gases by means of a fiber optic Fabry-Perot interferometer sensor', *Sensors Actuators, A Phys.*, vol. 118, no. 2, pp. 177–182, 2005.

[26] L. H. Chen, T. Li, C. C. Chan, R. Menon, P. Balamurali, M. Shaillender, B. Neu, X. M. Ang, P. Zu, W. C. Wong, and K. C. Leong, 'Chitosan based

fiber-optic Fabry-Perot humidity sensor', *Sensors Actuators, B Chem.*, vol. 169, pp. 167–172, 2012.

[27] Y. Zhao, R.Q. Lv, Y. Ying, and Q. Wang, 'Hollow-core photonic crystal fiber Fabry–Perot sensor for magnetic field measurement based on magnetic fluid', Optics & Laser Technology, vol. 44, no. 4, pp. 899-902, 2012.

[28] T. Wei, Y. Han, Y. Li, H. L. Tsai, and H. Xiao, 'Temperature-insensitive miniaturized fiber inline Fabry-Perot interferometer for highly sensitive refractive index measurement', Optics Express, vol. 16, no. 8, pp. 5764-5769, 2008.

[29] O. Frazão, S. H. Aref, J. M. Baptista, J. L. Santos, H. Latifi, F. Farahi, J. Kobelke, and K. Schuster, 'Fabry-perot cavity based on a suspended-core fiber for strain and temperature measurement', *IEEE Photonics Technol. Lett.*, vol. 21, no. 17, pp. 1229–1231, 2009.

[30] M. J. Gander, W. N. MacPherson, J. S. Barton, R. L. Reuben, J. D. C. Jones, R. Stevens, K. S. Ghana, S. J. Andersen, and T. V. Jones, 'Embedded micromachined fiber-optic fabry-perot pressure sensors in aerodynamics applications', *IEEE Sens. J.*, vol. 3, no. 1, pp. 102–107, 2003.

[31] J. Mathew, Y. Semenova, G. Rajan, and G. Farrell, 'Humidity sensor based on photonic crystal fibre interferometer', *Electron. Lett.*, vol. 46, no. 19, p. 1341, 2010.

[32] M. Hernaez, D. Lopez-Torres, C. Elosua, I. R. Matias, and F. J. Arregui, 'Sensitivity enhancement of a humidity sensor based on poly(sodium phosphate) and poly(allylamine hydrochloride)', *Proc. IEEE Sensors*, vol. 277, pp. 8264–8265, 2013.

[33] G. Jiménez-Cadena, J. Riu, and F. X. Rius, 'Gas sensors based on nanostructured materials', *Analyst*, vol. 132, no. 11, p. 1083, 2007.

[34] M. Stowell, J. M??ller, M. Ruske, M. Lutz, and T. Linz, 'RF-superimposed DC and pulsed DC sputtering for deposition of transparent conductive oxides', *Thin Solid Films*, vol. 515, no. 19 SPEC. ISS., pp. 7654–7657, 2007.

[35] M. Smietana, M. Sobaszek, B. Michalak, P. Niedzialkowski, W. Bialobrzeska, M. Koba, P. Sezemsky, V. Stranak, J. Karczewski, T. Ossowski, and R. Bogdanowicz, 'Optical monitoring of electrochemical processes with ITO-based lossy-mode resonance optical fiber sensor applied as an electrode', Journal of Lightwave Technology, 2018.

[36] J. Ascorbe, J. M. Corres, F. J. Arregui, and I. R. Matias, 'Humidity sensor based on bragg gratings developed on the end facet of an optical fiber by sputtering of one single material', Sensors, vol. 17, no. 5, pp. 991, 2017.

[37] C. Christopher, A. Subrahmanyam, and V. V. R. Sai, 'Gold Sputtered U-Bent Plastic Optical Fiber Probes as SPR-and LSPR-Based Compact Plasmonic Sensors', Plasmonics, pp. 1-10, 2017.

[38] Y. J. Rao, 'Recent progress in fiber-optic extrinsic Fabry-Perot interferometric sensors', *Opt. Fiber Technol.*, vol. 12, no. 3, pp. 227–237, 2006.

[39] Z. Wang, F. Shen, L. Song, X. Wang, and A. Wang, 'Multiplexed fiber fabry-perot interferometer sensors based on ultrashort bragg gratings', *IEEE Photonics Technol. Lett.*, vol. 19, no. 8, pp. 622–624, 2007.

[40] Y. Ou, C. Zhou, L. Qian, D. Fan, C. Cheng, and H. Guo, 'Large-capacity multiplexing of near-identical weak fiber Bragg gratings using frequency-shifted interferometry', *Opt. Express*, vol. 23, no. 24, p. 31484, 2015.

[41] R. Ryf, N. K. Fontaine, H. Chen, B. Guan, B. Huang, M. Esmaeelpour, A. H. Gnauck, S. Randel, S. J. B. Yoo, A. M. J. Koonen, R. Shubochkin, Y. Sun, and R. Lingle, 'Mode-multiplexed transmission over conventional graded-index multimode fibers', *Opt. Express*, vol. 23, no. 1, p. 235, 2015.

[42] H. Y. Fu, a C. L. Wong, P. a Childs, H. Y. Tam, Y. B. Liao, C. Lu, and P. K. a Wai, 'Multiplexing of polarization-maintaining photonic crystal fiber based Sagnac interferometric sensors.', *Opt. Express*, vol. 17, no. 21, pp. 18501–12, 2009.

[43] J.-W. Goossens, M. I. Yousefi, Y. Jaouën, and H. Hafermann, 'Polarization-Division Multiplexing Based on the Nonlinear Fourier Transform', vol. 25, no. 22, pp. 1–3, 2017.

[44] A. Lopez-Aldaba, D. Lopez-Torres, C. Elosua, J.-L. Auguste, R. Jamier, P. Roy, F. J. Arregui, and M. Lopez-Amo, 'Relative humidity multi-point optical sensors system based on fast Fourier multiplexing technique', in *Proceedings of SPIE - The International Society for Optical Engineering*, 2017, vol. 10323.

[45] Y. J. Rao, J. Jiang, and C. X. Zhou, 'Spatial-frequency multiplexed fiber-optic Fizeau strain sensor system with optical amplification', *Sensors Actuators, A Phys.*, vol. 120, no. 2, pp. 354–359, 2005.

[46] A. D. Wilson, and Baietto, M. 'Applications and advances in electronic-nose technologies', *Sensors*, vol. 9, no. 7, pp. 5099-5148, 2009.

[47] K. Arshak, E. Moore, G. M. Lyons, J. Harris, and S. Clifford, 'A review of gas sensors employed in electronic nose applications', *Sensor review*, vol 24, no. 2, pp. 181-198, 2004.

[48] C. Bariain, I. R. Matıas, C. Fernandez-Valdivielso, F. J. Arregui, M. L. Rodrıguez-Méndez, and J. A. De Saja, 'Optical fiber sensor based on lutetium bisphthalocyanine for the detection of gases using standard telecommunication wavelengths', *Sensors and Actuators B: Chemical*, vol. 93, no. 1-3, pp. 153-158, 2003.

[49] A. Lopez-Aldaba, A. M. R. Pinto, M. Lopez-Amo, O. Frazão, J. L. Santos, J. M. Baptista, H. Baierl, J. L. Auguste, R. Jamier, and P. Roy, 'Experimental and numerical characterization of a hybrid fabry-Pérot cavity for temperature sensing', *Sensors (Switzerland)*, vol. 15, no. 4, pp. 8042–8053, 2015.

[50] J. L. Santos, a P. Leite, and D. a Jackson, 'Optical fiber sensing with a low-finesse Fabry-Perot cavity.', *Appl. Opt.*, vol. 31, no. 34, pp. 7361–7366, 1992.

[51] D. Leandro, M. Bravo Acha, A. Ortigosa, and M. Lopez-Amo, 'Real-time FFT analysis for interferometric sensors multiplexing', *J. Light. Technol.*, vol. 8724, no. c, pp. 1–1, 2015.

[52] R. A. Perez-Herrera and M. Lopez-Amo, 'Fiber optic sensor networks', *Opt. Fiber Technol.*, vol. 19, no. 6 PART B, pp. 689–699, 2013.

[53] O. C. Akkaya, M. J. F. Digonnet, G. S. Kino, and O. Solgaard, 'Time-division-multiplexed interferometric sensor arrays', *J. Light. Technol.*, vol. 31, no. 16, pp. 3001–3008, 2013.

[54] R. Hernandez-Lorenzo, M. López-Amo, and P. Urquhart, 'Single and double distributed optical amplifier fiber bus networks with wavelength division multiplexing for photonic sensors', *J. Light. Technol.*, vol. 16, no. 4, pp. 485–489, 1998.

[55] A. Lopez Aldaba, D. Lopez-Torres, C. Elosua, J.-L. Auguste, R. Jamier, P. Roy, F. J. Arregui, and M. Lopez-Amo, 'SnO2-MOF-Fabry-Perot optical sensor for relative humidity measurements', *Sensors Actuators, B Chem.*, vol. 257, pp. 189–199, 2018.

[56] N. G. Patel, P. D. Patel, and V. S. Vaishnav, 'Indium tin oxide (ITO) thin film gas sensor for detection of methanol at room temperature', *Sensors Actuators, B Chem.*, vol. 96, no. 1–2, pp. 180–189, 2003.

[57] W. Schmid, 'Consumption measurements on SnO2 sensors in low and normal oxygen concentration', *Diss. am Inst. für Chemie und Pharm. der Eberhard-Karls- Univ. Tübingen*, 2004.

[58] D. Lopez-Torres, C. Elosua, J. Villatoro, J. Zubia, M. Rothhardt, K. Schuster, and F. J. Arregui, 'Enhancing sensitivity of photonic crystal fiber interferometric humidity sensor by the thickness of SnO2 thin films', *Sensors Actuators, B Chem.*, vol. 251, 2017.

[59] M. Bravo, M. Fernández-Vallejo, M. Echapare, M. López-Amo, J. Kobelke, K, Schuster 'Multiplexing of six micro-displacement suspended-core Sagnac interferometer sensors with a Raman-Erbium fiber laser' *Optics express* vol. 21, no. 3, pp.2971-2977, 2013.

[60] P. Childs, 'An FBG sensing system utilizing both WDM and a novel harmonic division scheme', *J. Light. Technol.*, vol. 23, no. 1, pp. 348–354, 2005.

[61] J. Mizsei, 'How can sensitive and selective semiconductor gas sensors be made? ', *Sensors and Actuators B: Chemical*, vol. 23, no. 2-3, pp. 173-176, 1995.

[62] C. Delpha, M. Siadat and M. Lumbreras, 'Discrimination of a refrigerant gas in a humidity controlled atmosphere by using modelling parameters', *Sensors and Actuators B: Chemical*, vol. 62, no. 3, pp. 226-232, 2000.

[63] X. Wang, N. Miura and N. Yamazoe, 'Study of WO3-based sensing materials for NH3 and NO detection', *Sensors and Actuators B: Chemical*, vol. 66, no. 1-3, pp. 74-76, 2000.